DWPF Melter Air-Lift Bubbler:

Physical Testing with Glycerin

UNCLASSIFIED
DOES NOT CONTAIN
UNCLASSIFIED CONTROLLED
NUCLEAR INFORMATION

ADC &
Reviewing
Official: _____
(Name and Title)

Date: _____12/17/02_____

SAFETY · RESPONSIBILITY · SECURITY

SRS

SAVANNAH RIVER SITE

Westinghouse Savannah River Company
Savannah River Site
Aiken, SC 29808
January , 2003

WSRC-TR-2002-00421 Rev. 0

DWPF Melter Air-Lift Bubbler:

Physical Testing with Glycerin

SAVANNAH RIVER TECHNOLOGY CENTER

Hector N. Guerrero

Dennis F. Bickford

DOCUMENT: WSRC-TR-2002-00421 Rev. 0

TITLE: DWPF Melter Air-Lift Bubbler:

Physical Testing with Glycerin
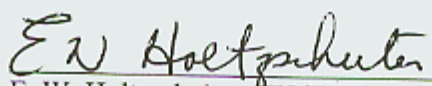
APPROVALS:

Hector N. Guerrero   Date: _10/21/02_
Hector N. Guerrero, Author (ETF/EDS/EES)

Dennis F. Bickford   Date: _10/22/02_
D. F. Bickford, Author (ITBD/ITS/WTT)

D. Burns   Date: _10/30/02_
D. Burns, ETF/EDS/EES Manager

R. H. Spires   Date: _10-21-02_
R. H. Spires, ITBD/ITS/WTT Manager
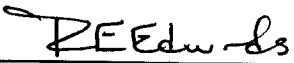
E. W. Holtzscheiter   Date: _10-21-02_
E. W. Holtzscheiter, ITS/WTT Manager

Mark R. Duignan   Date: _10/21/02_
M. R. Duignan., Technical Reviewer, ETF/EDS/EES

DOCUMENT: WSRC-TR-2002-00421 Rev. 0

TITLE: DWPF Melter Air-Lift Bubbler:

                    Large Scale Model Testing in Glycerin

APPROVALS (Continued):

_REEdwards_____ Date: 12/11/02

R. E. Edwards, Jr., Mgr. (PE/WDED/HLWCE)

_BLLewis_____ Date: 12/6/02

B. L. Lewis, Mgr. (PCE/WDED/HLWCE)

Table of Contents

List of Figures

List of Tables

1.0 Executive Summary

Development of the Airlift Bubbler was initiated as part of a DOE Tank Focus Area program to assess possible means of increasing Defense Waste Processing Facility Melter melt rate in FY01. Analysis of the DWPF Melter thermal performance over its operating history since 1997 and three batch feeds, using a lumped parameter model, indicated that electrode power was continuously decreasing due to a thermal resistance layer in the cold cap. This thermal resistance layer may consist of a foamy layer or crystalline layer or both. Thus, while electrode capacity was more than adequate, it could not be increased due to overheating. Furthermore, dome heater power, which has been used to compensate for reduced electrode power, has been significantly reduced due to the loss of one dome heater. Consequently, melt rate has been reduced 50% from its historic maximum. Bubblers were considered as a means of increasing glass circulation and opening a vent in the cold cap to allow increased electrode power. Radiant heat from this vent would supplement the reduced dome heater power and thus increase the present melter capacity. An innovative bubbler system, using the airlift principle, has been designed for installation through the DWPF melter top head. The Airlift Bubbler has significant advantages over conventional bubblers in that a measurable flow of hot glass is actually pumped within the bubbler tube from lower elevations in the melter to surface layers adjacent to the cold cap for gross melter circulation and improved heat transfer. Conventional bubblers where bubbles outside the bubbler tube basically only provide local agitation.

Previous development efforts (Ref. 1) include a half-length airlift used with glycerin to develop a proof-of-principle design, and an Inconel proof-of principle airlift tested in molten glass. Tests have shown the Airlift Bubbler to be an effective pump. A three-inch inside diameter unit was found to pump approximately 1.5 tons of molten glass per hour, at a pump head height of eleven inches. Pumping rate was controlled by varying air flow rate to the airlift. Prior experience with traditional bubblers in glass, and evaluation of this performance with the lumped parameter heat transfer model indicates that melt rate increases of 10-30% or higher can be expected from a single unit.

The current developmental program focuses on design and testing of a prototype Airlift Bubbler that addresses installation and operational issues in the DWPF Melter. A full-scale unit will be installed in the glass hold tank of the DWPF Pour Spout Test Stand at Clemson University, and used for airlift life testing. This report is concerned with physical model testing with glycerin to investigate design details influencing glass-flow, and the effect of airlift pumping on the circulation of the melter. The glycerin tests provide systematic evaluation of airflow rate, bubbler submerged depth, nozzle design and number, and glass discharge elevation.

Testing results are summarized as follows:
- A Plexiglas model of the Prototype Airlift Bubbler with an internal I.D. of 2.4-inches was tested in a tank, 3 ft. square by 3 ft. high, of chilled glycerin to simulate glass. Test parameters were varied over the ranges: liquid viscosities from 15 - 72 poise; air flows from 0.2 –1.8 scfm; submerged depths from 14 - 29 inches; and discharge heights from 6 inches below to 9-inches above the liquid surface.

- At typical conditions of 60 poise, 1.2 scfm air flow, 25-inches submerged depth, and 4-inch discharge height, the liquid pumping rate was 0.285 ft^3/min., or an equivalent glass capacity of 2600 lbs./hr.

- The pumped liquid flow increased monotonically with air flow for the air flows used. At the maximum air flows, the bubbles were still distinctly separate, being in the slug flow regime. A turning down of the liquid flow vs. air flow curve was evident when the flow pattern became disorganized or churn-flow at the high air flows. At somewhat higher air flows than those used in these tests, annular flow would be reached and very little liquid flow would be pumped.

- Increasing the bubbler submerged depth increases the liquid pumping rate for the same airflow rate. This is due to the increased static pressure driving head of the two- phase mixture. Increasing the bubbler discharge height above the liquid surface reduces the pumped liquid flow. This is due to the increase an additional static head above the liquid that must be overcome.

- The number of nozzles from 1 to 6 has no effect on the liquid flow. Thus limiting the nozzles to 2 (for some redundancy) would result in a simpler design and increased flow area.

- Tank flow circulation patterns, visualized by minute entrained air bubbles, plastic particle tracers, and colored dye, show that the bubbler "zone of influence" basically covers the entire tank to a diameter of 3 ft. and depth of 6-12 inches below the bubbler opening.

- The outlet flow pattern at the liquid surface suggests a butterfly shaped region or two oval areas opposite the two outlet slots. Locating the bottom of the exit slots below the surface of the liquid appears to provide a beneficial horizontal momentum to the liquid. The escaping bubble tends to expand and burst outside of the slots and pushes the liquid outward, increasing the extent of the "zone of influence" and improving convection under the cold cap.

Anticipated benefits to DWPF of the airlift bubbler are:
- Enhanced melt rate from direct action of increased overall glass circulation rates improving transfer of electrode power to the bottom of the cold cap. This may be the result of increased overall glass velocity or improved venting of cold cap gases trapped under the cold cap. This effect is estimated at about 10% up to 30% increase per airlift (flange).

- Additional increases to melt rates from enhanced power available to the cold cap and slurry indirectly by radiant heat transfer from a vent or melted glass surface to the melter plenum. This effect is projected to provide a melt rate increase of up to 20% per airlift (flange). It increases total power available to the melter by allowing additional electrode power to be applied without increasing the glass temperature beyond the set point limit.

- More uniform glass pool temperatures, making it easier to stay within temperature operating limits at the top and bottom of the glass pool.

- Evaluation of the heat transfer across the surface of the glass in DWPF suggests that a foamy crystalline layer may be forming. By pumping hot glass to the cold cap region and its improvement of the global tank circulation, the airlift may help dissolve or dissipate these un-dissolved crystalline materials.

2.0 Introduction and Summary

The DWPF Melter has recently experienced a number of operational problems that seriously eroded the capability to produce HLW canisters. A 20% reduction in electrode power, apparently due to a crystalline layer under the cold cap, was experienced with the new Macrobatch 3 feed relative to Macrobatch 2. This could only be compensated by an increase in dome heater power to maintain total melter power. However, now one of the four dome heaters has failed, limiting the feed rate to 0.35 gpm, a 36% reduction from Macrobatch 2. DWPF Melter canister production rate also decreased with Macrobatch 2 relative to Macrobatch 1 by approximately 23%. This might be attributed to (1) a higher foam generation in Macrobatch 2 that diminished heat transfer and (2) higher glass viscosity that reduced melter flow recirculation.

DWPF is considering a number of options to increase the meltrate, one of which is the Airlift Bubbler. The Airlift Bubbler, under TFA sponsorship, is being developed to increase melt pool circulation as a means to improve meltrate. It is basically an airlift pump that brings hot glass from lower melt pool elevations to the cold cap region, melting part of the cold cap. This also results in opening of a vent hole that provides radiant heat to the upper plenum to supplement dome heater power. Thus electrode power can be increased to compensate for the power lost due to the failed dome heater.

Bubblers that pump glass through the airlift principle can increase the overall melter circulation rate. The higher circulation rate would increase the film heat transfer coefficient to the cold cap (to compensate for the foam thermal resistance) by bringing more hot glass from lower elevations. Also by maintaining a high temperature at the uncovered glass surface, radiation to the upper plenum, which is reflected back to the top of the cold cap, provides more heat to dry and calcine the slurry prior to melting. During normal melting and idling conditions, the uppermost glass in the glass pool is cooler than the nominal melting temperature. Thus, pumping hot glass to this level (underneath the surface) may help to dissolve any layers that form, and restore any local composition differences resulting from accumulations or local volatilization.

The Plexiglas bubbler is a model of the prototype Inconel Airlift Bubbler being fabricated to be used in life testing with molten glass. It has an internal bore of 2.5-inches and inserts to simulate 2 bore protrusions associated with internal air passages built into the wall of the housing. The bore diameter was dictated by the available nozzle opening and wall thickness to allow for erosion. There is no separate air tube as in the proof-of-principle bubbler (Ref. 1). For the Plexiglas model, it was not necessary to simulate the internal air passages. A row of 6 nozzles, above the open bottom end of the bubbler tube, injects air bubbles into the liquid inside the bubbler tube. The rising air bubbles produce a two-phase mixture, which has a lower fluid density than the fluid outside the bubbler. Thus a pressure difference between outside and inside

regions to induce flow up from the open bottom end of the tube, then out of the upper pair of slots.

The model airlift bubbler was installed inside a tank with glass and clear lexan sides, 3ft square by 4ft high. The tank was filled with glycerin to a depth of 3 ft. The glycerin temperature was varied from room temperature, 21^oC to 5^oC, varying the viscosity from 15 poise to 72 poise. The bubbler initially had an available submergence depth (distance from its bottom opening to the liquid surface) of 29-inches. By moving the bubbler up or down, the submergence depth could be adjusted. A flow catcher with calibrated orifices was installed about the bubbler exit slots to measure the exiting liquid flow. This generally required a lift (distance from the bottom of the exit slots to the liquid surface) of at least 4-inches. For some tests, the slots were lengthened to determine the effect of short submergence depths.

Testing results are summarized as follows:

The pumped liquid flow increased monotonically with airflow for the range of airflow used. At the maximum airflows tested, the bubbles were still distinctly separate, and observed as cylindrical bubbles that spanned the bubbler inside diameter between liquid slugs. A leveling off of the flow was evident when the flow pattern became disorganized or churn-flow.

At typical conditions of 60 poise, 1.2 scfm airflow, 24-inches submerged depth, and 4-inch discharge height, the liquid pumping rate was 0.285 ft^3/min., or an equivalent glass capacity of 2600 lbs./hr. Melter operating flows will depend on expected erosion rates to be determined from glass tests with an Inconel bubbler.

Increasing the bubbler submerged depth increases the liquid pumping rate for the same airflow rate. This is due to the increased static pressure driving head of the two-phase mixture. Increasing the bubbler discharge height over the liquid surface reduces the pumped liquid flow. This is due to the increase of an additional static head above the liquid that must be overcome.

The number of nozzles from 1 to 6 has no significant effect on the liquid flow. Thus limiting the nozzles to 2 (for some redundancy) would result in a simpler design and increased flow area.

Tank flow circulation patterns, visualized by minute entrained air bubbles, plastic particle tracers, and colored dye, show that the bubbler "zone of influence" basically covered the entire 3 ft. square tank and to a depth of 6-inches to a foot below the bubbler opening. This was observed even with airflows as low as 0.3 scfm.

The outlet flow pattern at the liquid surface is in the shape of two oval areas opposite the two outlet slots. Locating the bottom of the exit slots below the surface of the liquid appears to provide a beneficial horizontal momentum to the liquid. The escaping bubble tends to expand and burst outside of the slots and pushes the liquid outward. The increased momentum extends the area of influence of the bubbler at the upper layers and increases convection under the cold cap. Lowering the slots by more than 2-inches however reduces the maximum bubbler flow.

A design equation, based on a momentum balance between the static pressure driving head and the frictional pressure drop, was confirmed experimentally. This relates the effects of gas flow, insertion depth, lift, hydraulic diameter, and viscosity on the pumped liquid flow. A total of 104 data points were used in the correlating equation, representing flows from 0.2 scfm to 1.8 scfm, liquid viscosities from 15 poise to 72 poise, insertion depths of 14 inches to 29-inches, and lifts from 0 to 9 inches, with a correlating parameter of R^2=0.78

Implications of the use of an Airlift Bubbler on available power in the DWPF Melter may be assessed as follows: Assume a nominal glass flow of 2000 lbs/hr that may reduce erosion to acceptable values, a lower glass temperature of 1100°C and a glass surface temperature of 850°C (as suggested by lumped parameter model results). This represents a power flow from the electrodes to the upper plenum by radiant heat of 88 kW, which is additional power to increase melt rate.

3.0 Objectives

The objectives of the Airlift Bubbler Physical Testing are to investigate the flow characteristics of the bubbler as an aid to finalize the prototype bubbler design, including:

- flow characteristics at the outlet slots of the bubbler, the foam propagation at the surface of the glycerin, flow circulation patterns in the tank, as well as bubble patterns in the tank.
- effects of airflow rate, depth of insertion, and height of the bottom ends of the outlet slots above or below the glycerin surface on the pumping capacity of the airlift.
- effect of viscosity, nozzle plugging and other operational issues.

4.0 Airlift Bubbler Model Description

A comprehensive description of the Airlift Bubbler, or Airlift for short, and previous testing is given in Reference 1. In those tests, a short 14-inch long 3-inch ID plastic bubbler was tested in glycerin and a full length, 3-inch ID Inconel bubbler was tested in glass. The present Plexiglas Airlift Bubbler model is used for flow visualization tests in glycerin and has prototypical inside dimensions of the Inconel Airlift to be designed for installation in the DWPF Melter. Figure 1a is an overall photograph of the Plexiglas model and Figure 1b is a close up view of the lower end and nozzles. Figure 2 provides the design details of the Plexiglas model.

The Airlift is essentially an air pump consisting of a vertical 2.5-inch ID pipe with bottom and top openings, which is immersed into a pool of liquid. Its operation can be understood by reference to the schematic diagram of Figure 3. The airlift bubbler is installed inside a large 200 gallon tank of glycerin. Air is injected into the lower region of the bubbler through nozzles located slightly above the bottom opening. Air bubbles are generated at the nozzles and rise through the liquid. These rising air bubbles create a two-phase mixture, which draws in liquid through the bottom hole opening by virtue of the difference in densities inside and outside of the Airlift. The liquid then exits through the slots at the upper end of the tube and the air bubbles separate and escape to the atmosphere above the liquid surface. Thus, liquid from the lower layers of the tank is pumped to the upper region of the pool.
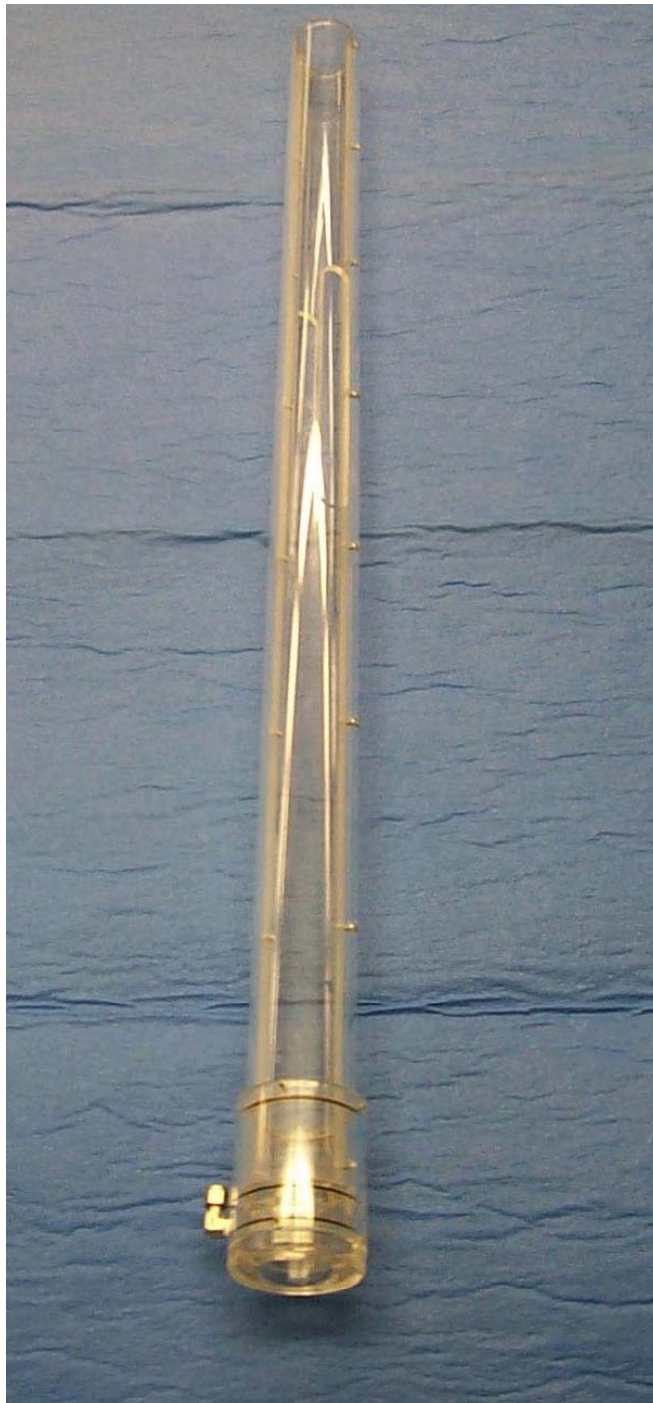
(a)

(b)

Figure 1 Photograph of Plexiglas Airlift Bubbler Model
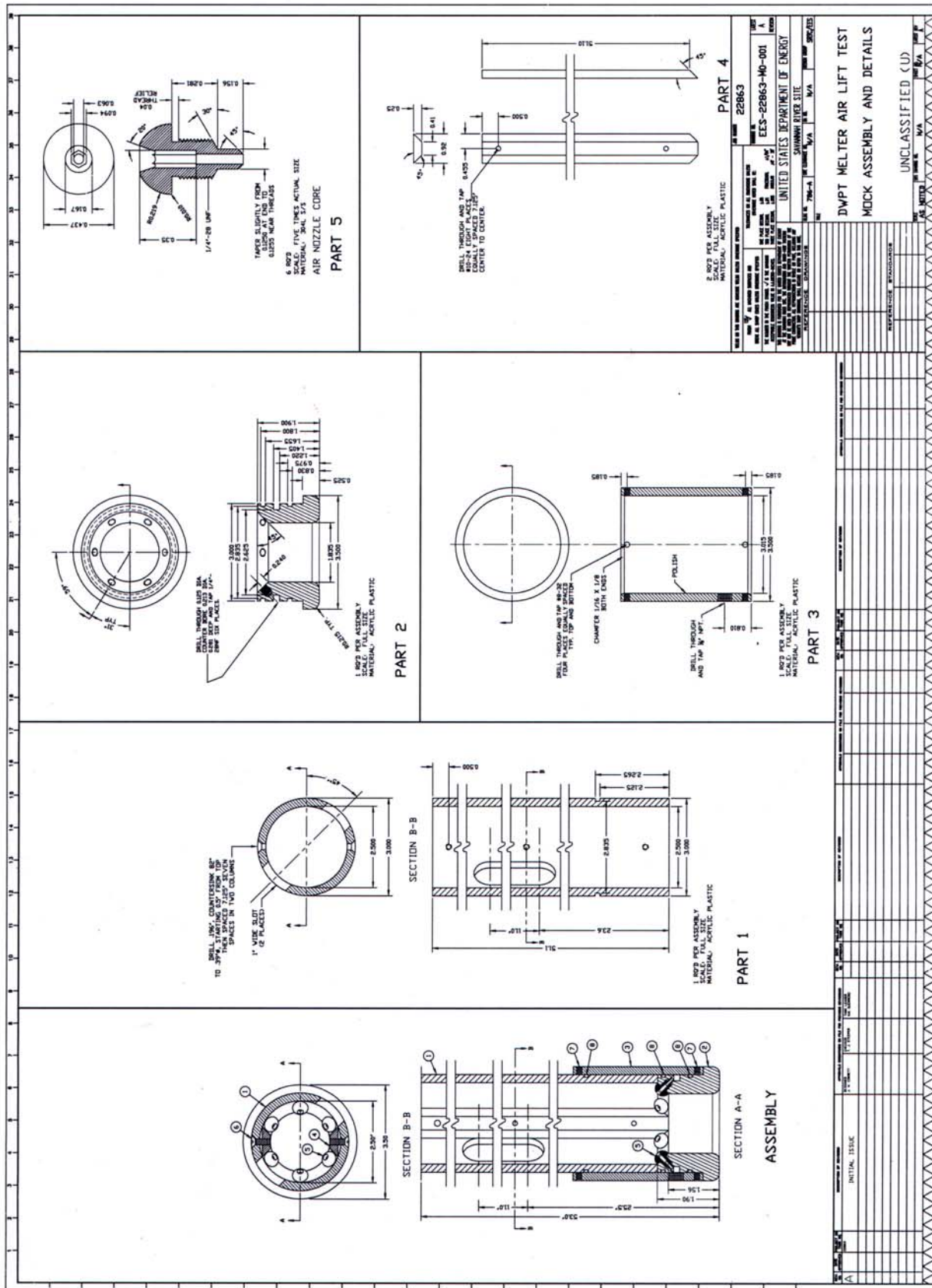
Figure 2   Plexiglas Airlift Bubbler Model Dwg. EES-22863-M0-001
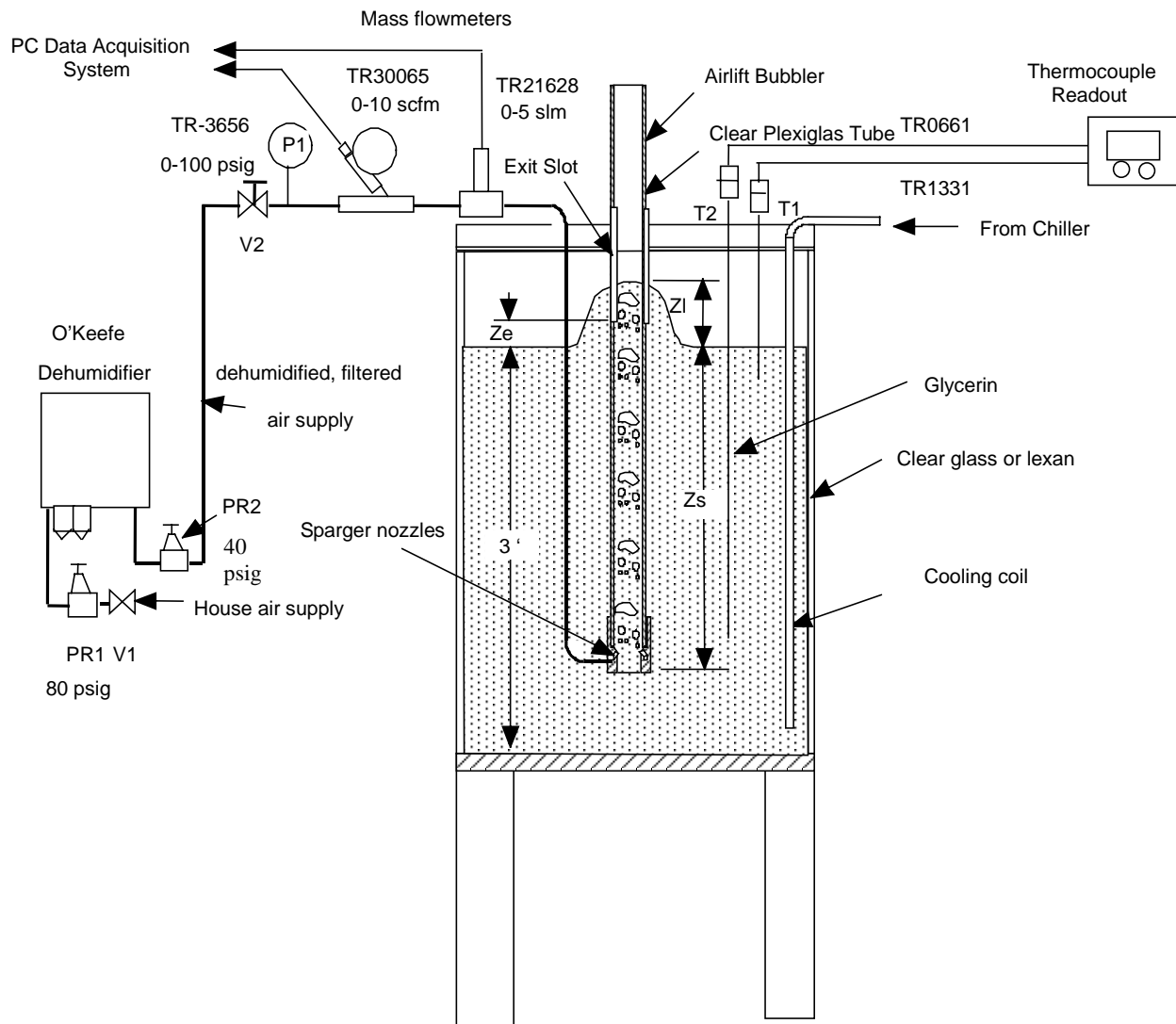
Figure 3   Airlift Bubbler Model Test Rig for Glycerin Testing

Figure 4 Photograph of Plexiglas Airlift Bubbler Model Test Rig.

5.0   Airlift Bubbler Model Testing Procedure

5.1   Plexiglas Airlift Bubbler Model Test Rig

The Plexiglas Airlift Bubbler Model Test Rig is shown in the photograph of Figure 4 during construction. The glycerin tank has 3ft. sides and a height of 4 ft. It is filled with glycerin to a depth of 3 ft. The transparent side walls are made of 1-inch thick tempered glass on 3 sides and 1-inch thick Plexiglas on the fourth side. Copper cooling coils are installed along two side walls and these are connected to the building chiller to control the glycerin temperature which must be cooled down to 7^oC to simulate a glass viscosity of 60 poise. Aluminum foil backed styrofoam panel insulation was used on all sides to achieve reasonable cool down rates. One panel was then removed for viewing.

Instrumentation for the test included an air mass flow meter to measure the gas flow rate, pressure transducer to measure the gas pressure before the nozzles, and two thermocouples.   The cooling coils resulted in an almost linear temperature gradient that typically increased from 6.75^oC from the bottom of the tank to 20^oC at the glycerin surface. Consequently, one thermocouple T1 was installed inside the flow catcher. The other thermocouple T2 was installed at the same elevation as the bottom hole opening. During Airlift operation, both thermocouple readings were close to each other. T2 temperature readings were used as representative of the glycerin temperature inside the bubbler since it directly measured the glycerin flow temperature. All sensors were connected to a PC based data acquisition system.
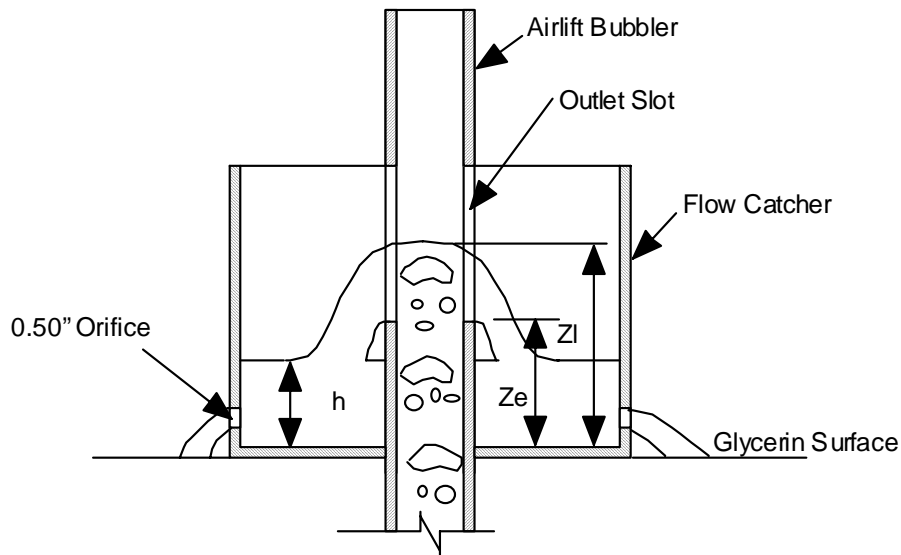
Figure 5   Flow Catcher Diagram

The liquid flow inside the Airlift Bubbler was measured directly, using a Flow Catcher that contained the glycerin flowing out of the exit slots. Figure 5 shows a schematic of the Flow Catcher, which is positioned so that a steady liquid level is maintained below the bottom of the exitt slots. The liquid level is maintained by a steady outflow through eight 0.50-inch diameter flow orifices. The flow calibration of the orifices was previously obtained in Ref. 1 using near

room temperature glycerin and 100 poise silicone oil. This calibration was checked during the present testing at the actual glycerin temperatures used (7°-16°C). This was done by catching the flow again out of the orifices and using the volume-time method. Both sets of data were then combined (Figure 6) to give a coefficient of discharge, *Cd*, equation for the ½ inch orifice as,

$$C_d = 0.119\sqrt{\mathrm{Re}_o}$$
$$Q_l = C_d\sqrt{2gh}A_o$$

where Re_o is the orifice Reynolds number, Q_l is the volumetric flow rate, g is gravitational constant, h is the liquid level height from the centerline of the orifice, and A_o is the orifice area.

Orifice Calibration
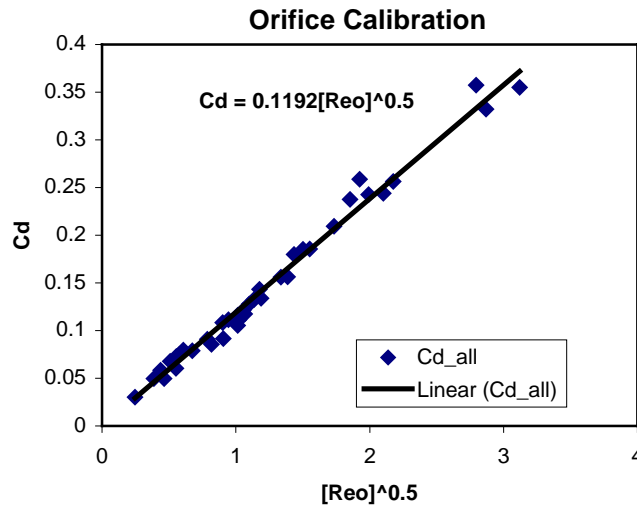
Figure 6   Flow Catcher Orifice Calibration

5.2 Testing Procedure

Test conditions were attained when thermocouple T2, adjacent to the bubbler opening, indicated the desired temperature setting. Air was then injected through the nozzles. A number of tests were conducted to determine:

- the bubble flow pattern as a function of air flow and the number of nozzles,
- flow circulation pattern in the tank, as shown by entrained air bubbles and short (1/16") lengths of 1/16" diameter plastic rods, which are neutrally bouyant,
- outlet flow pattern as a function of height of the bottom of the outlet slots above or below the glycerin surface,
- liquid pumping rates as a function of air flow, liquid viscosity, depth of insertion, bubbler length between inlet and outlet slot bottom, and
- length of time required to blow liquid from the air line.

For the tests investigating the outlet flow pattern, the Flow Catcher was removed.

6.0 Test Results

6.1 Theoretical Considerations

To evaluate parameter effects, as stated in the Objectives, Section 3, the data will be examined in relation to a model, previously discussed in Ref. 1. This model, after verification with the glycerin data, can then be used to scale up to glass conditions or for any deviations in the present Airlift bubbler design. Referring to Figure 3, the important parameters are submergence depth, Z_s, lift, Z_l, and void fraction, α. Applying the momentum equation, [1] is obtained.

$$\rho g Z_s = \rho g (1-\alpha)(Z_s + Z_l) + \frac{(1-\alpha) f \rho J_m^2 (Z_s + Z_l)}{2D} \quad . \qquad [1]$$

Here, ρ is the liquid density; g is gravitational acceleration; α is the void fraction; Z_s is the submerged depth; Z_l is the lift or height of the two-phase mixture above the surface of the liquid; D is the hydraulic diameter of the bubbler; and J_m is the mean mixture velocity. Assuming a homogenized flow, J_m is the sum of the liquid and gas superficial velocities, J_l and J_g, respectively. The superficial velocities are defined:

$$J_l = \frac{Q_l}{A_b}$$

$$J_g = \frac{Qg}{A_b}$$

where Q_l and Q_g are the liquid and gas volumetric flow rates, and A_b is the bubbler flow area. The friction factor may be given by a generalized Reynolds number equation

$$f = \frac{C}{\text{Re}^n} \qquad [2]$$

where Re is based on J_m and D..

Equation [1] may be rewritten,

$$\Delta p_s = \alpha \rho g Z_s = \rho g (1-\alpha) Z_l + \frac{(1-\alpha) f \rho J_m^2 (Z_s + Z_l)}{2D} \qquad [1a]$$

where Δp_s is the static pressure driving head due to bubbler submergence which is balanced by the static pressure due to lift (first term on the right) and the frictional pressure drop (second term). A second relation is available from the Drift Flux equation, which has been found (Ref. 4) to characterize bubbly and slug flow, as given in [3].

$$\frac{J_g}{\alpha} = C_o (J_g + J_l) + V_t \qquad [3]$$

where C_o is a distribution parameter and V_t is the bubble velocity relative to the average mixture velocity, called the drift or terminal velocity. For turbulent flow, C_o=1.26, and for laminar flow C_o=2.28 (Ref. 3). This equation expresses the phase velocity of the gas (left hand side) as the sum of the mixture velocity and the gas terminal velocity, V_t in still liquid.

Combining [1] and [3], a correlating equation for the liquid flow as a function of gas flow, bubbler parameters, and liquid physical properties, may be obtained as:

$$J_g = [C_o J_m + V_t)][1 - \frac{Z_s}{(Z_s + Z_l)(1 + \frac{fJ_m^2}{2gD})}] \qquad [4]$$

Here, the liquid superficial velocity is a function only of the gas superficial velocity, liquid properties, bubbler submergence and lift, and the terminal velocity. The void fraction is implicit in the terminal velocity, which must be obtained from an experimental correlation.

6.2   Bubble Flow Patterns Inside Airlift Bubbler

Figures 7a and 8a[1] show the bubble flow pattern inside the bubbler at a gas flow rate of 0.2 scfm at 21°C and 7°C, respectively. In Figures 7a-7e, two of the six available nozzles were open, and in Figures 8a-8e, one nozzle was operating. For the multiple nozzle arrangement (See also Figures 9 and 10), the bubbles departing from the nozzle quickly combine above the nozzles into a single bubble. A train of distinct single bubbles then rises up through the bubbler riser passage. At a flow of 0.2 sfm, these bubbles are small and almost spherical, typically 1.4-inch diameter at both temperatures. At this flow however, there is a small net liquid flow out of the exit slots. Also, there are small air bubbles between the large bubbles which flow downwards, which indicate some recirculation downwards of the liquid near the walls. These small bubbles are more numerous at the higher temperature.

At a flow of 0.4 scfm, the air bubbles get bigger in diameter and are oblate-spheroidal in shape. Ar 21°C, the bubble diameter is typically 1.7-inches, while at 7°C, the bubbles grow to almost fill the ID of the bubbler (2-inch ID). The bubble lengths are about 2 inches at 21°C and 3.5 inches at 7°C. At these flows the bubbles are still distinct entities and the bubbles rise in a regular consistent spacing. The bubble spacing is closer at the lower temperature.

At higher flows, the bubbles grow to about 2-inches (distance between the inner wall protrusions). The bubbles are longer and more closely spaced at 7°C than at 21°C. This behavior can be attributed to the slower bubble rise velocities and lower liquid velocities at the lower temperature (higher viscosity). This leads to higher void fractions at high viscosity compared to low viscosity for the same gas flow.

---

[1] The photographs of the moving bubbles in these and succeeding figures were made from digital video tape, and do not have as good a resolution as that from a still photograph. As tests progressed, small entrained bubbles tended to accumulate and obscure the larger bubbles.

(a)
0.2 scfm

(b)
0.4 scfm

(c)
0.6 scfm

Figure 7 Bubble Flow Patterns at 21°C

(a)
0.2 scfm

(b)
0.4 scfm

(c)
0.6 scfm

Figure 8 Bubble Flow Patterns at 7°C

(d)
0.8 scfm

(d)
0.8 scfm

(e)
1.0 scfm

(e)
1.0 scfm

Figure 7 (cont'd.) Bubble Flow Patterns
at 21°C, 2 nozzles

Figure 8 (cont'd.) Bubble Flow Patterns
at 7°C, 1 nozzle

Above the nozzles, there is a tendency for a bubble to catch up with the preceding bubble and coalesce, as shown in Figure 9a. This leads to longer bubbles and longer spacings (Figure 9b). This however appears to be random and averaged over a short period, the liquid flow is relatively constant for a given gas flow.

(a) 0.2 scfm, 12°C   (b) 0.4 scfm, 12°C

Figure 9 Coalescence of Bubbles

(a) 0.4 scfm, 7°C, 2 Nozzles   (b) 0.4 scfm, 7°C, 6 Nozzles

Figure 10 Effect of Number of Nozzles

The effect of the number of nozzles on the flow pattern is shown in Figures 8b, 10a and 10b for 1, 2, and 6 nozzles, respectively. For the same gas flow and temperature (0.4 scfm, 7°C), the bubbles appear to grow larger as the number of nozzles increase. However, there is no significant difference in measured liquid flows, within the experimental error. (See Fig. 20.)

6.3 In-tank Flow Distribution

The extent of the flow recirculation zone inside the tank affected by the Airlift Bubbler was made evident by small entrained air bubbles generated as a result of liquid flowing back into the glycerin surface. Figure 11 shows that for an air flow of 0.8 scfm, 5.4^{o}C, this recirculation zone is a cylindrical volume extending to the side walls (3 ft. dia.), from the glycerin surface to 6-inches below the bubbler opening. The flow catcher was not installed in this case so that the outlet flow was freely flowing through the two exit slots. Notice the butterfly flow pattern at the top surface of the glycerin.

Figure 11 In-tank Flow Distribution Shown by Entrained Air Bubbles

(0.8 scfm, 5.4^{o}C, Slots 1-inch above Surface)

In another test, red food coloring was injected into the outlet flow of the bubbler. Figure 12 shows for a flow of 0.5 scfm at 7.2^{o}C, the extent that the dye reached horizontally at the surface, then down into the tank, and finally radially into the bubbler opening.
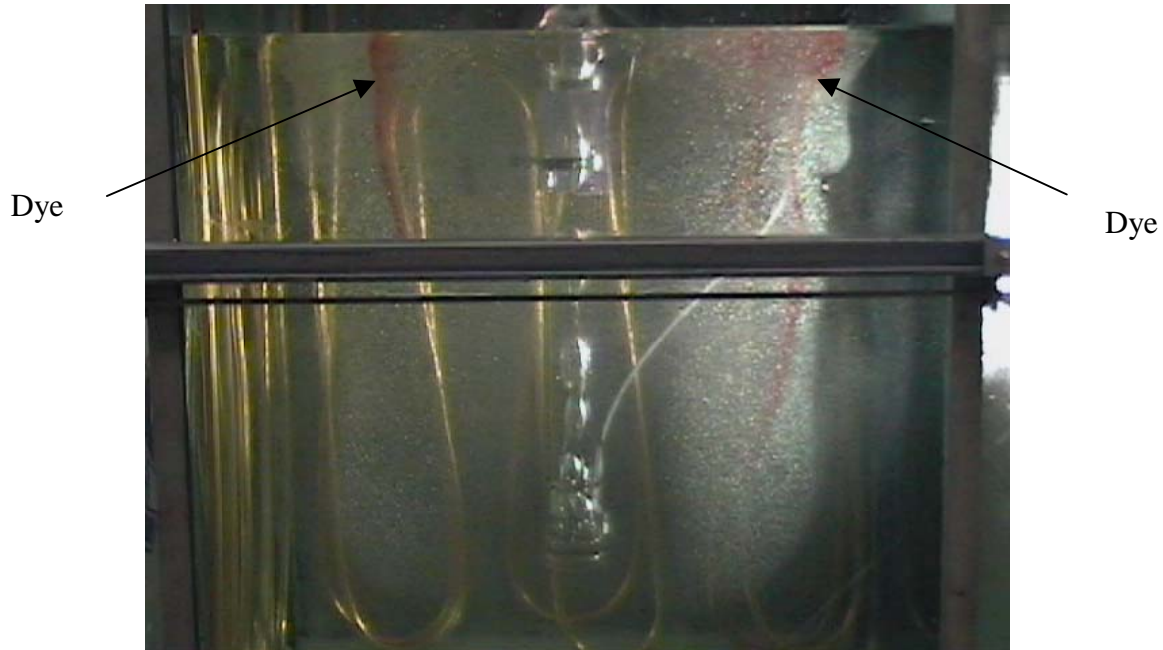
Figure 12   In-Tank Flow Distribution Shown by Red Food Coloring
(0.5 scfm, 7°C, Exit Slot 2-inches Below Surface)

6.4 Effect of Exit Slot Elevation

The effects of the location of the exit slots relative to the liquid surface are shown in Figure 13 to 17.

Bottom of Slots Level with Glycerin Surface
Figures 13 and 14 show the outlet flow coming out of the two slots for two air flows. Notice the elongated, bubbly flow influenced region on either side of the slots. The bubbles lift the liquid 1.5-inch for a gas flow of 0.3 scfm and about 3-inches for a gas flow of 1.0 scfm). A strong component of down flow is apparent for the higher liquid flow.

Bottom of Slots 4-inches Below Glycerin Surface
Figure 15 shows the overall tank flow distribution with entrained gas bubbles and red food coloring. The whole tank is basically involved in the flow recirculation. Of special interest is the expansion of the outgoing bubble through the slots while still below the surface (See also Figure 12).

Exit flow
influenced
region

Exit flow
influenced
region
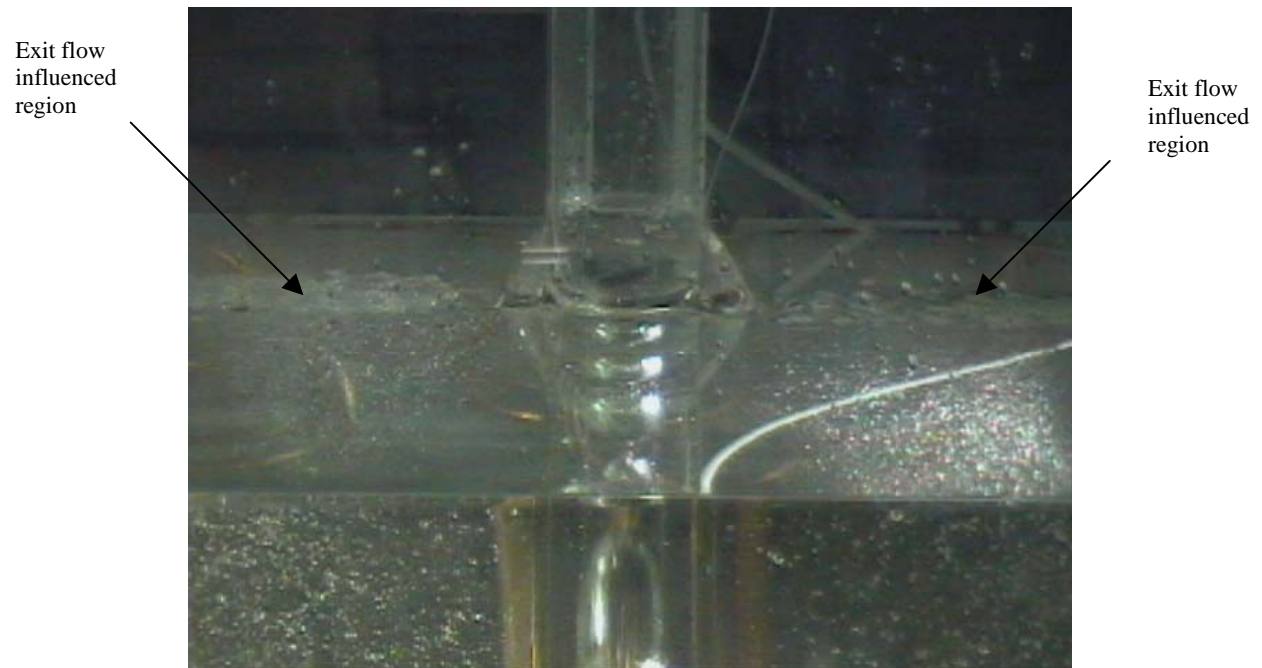
Figure 13 Outlet Flow Pattern with Slot Bottoms Level with Surface (0.3 scfm, 7.8^{o}C)

Figure 14 Outlet Flow Pattern with Slot Bottoms Level with Surface (1.0 scfm, 5.6^{o}C)

Dye
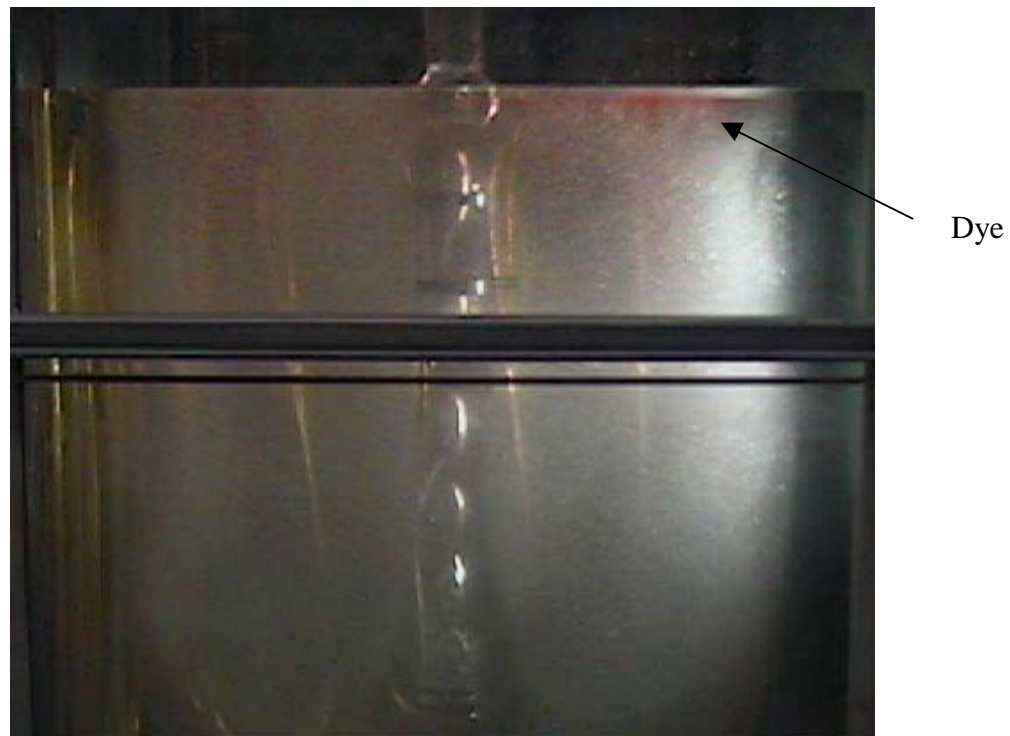
Figure 15   In-Tank Flow Distribution with Exit Slot Bottoms 4-inches Below Surface
(0.48 scfm, 6°C)

Expanding bubble

Figure 16 Outlet Flow Pattern with Exit Slot Bottom 6-inches Below Surface
(0.3 scfm, 5.7°C)

Figure 17 Outlet Flow Pattern for Exit Slot Bottoms 4-inches Above Surface
(0.3 scfm, 5.7^{o}C)

Bottom of Slots 6-inches Below Glycerin Surface
Figure 16 gives a view of the glycerin top surface with the bottom of the exit slots 6-inches
below the surface. A large air bubble is forming outside the bubbler on the left side. The gas
bubble expanded and escaped through the slot opening below the surface in a similar manner as
in Figure 15. What is interesting are the wave fronts ahead of the gas bubble, left by previous
bubbles. This indicates that a strong horizontal flow component is induced when the slot
bottoms are below the surface, as in Figure 11 and 12 when the slots are 1-inch and 2-inches
below the surface, respectively. However the longer submerged slots present a larger hydraulic
resistance to the exit flow.

Bottom of Slots 4-inches Above Glycerin Surface
Figure 17 shows a horizontal view of the outlet flow pattern when the exit slot bottoms are 4-
inches above the liquid surface. Here, a gas bubble has just burst inside the bubbler upon
reaching the slot bottom elevation. Two other bubbles in the bubble train are shown. At this gas
flow of 0.3 scfm, the liquid just flows along the outside wall of the bubbler. Thus, there is a low
horizontal flow component near the surface. Further, the high lift distance above the surface
reduces the overall liquid flow, as indicated by the data (See Figure 19).

6.5 Correlation of Liquid Flow Capacity

6.5.1 Effect of Liquid Viscosity and Submergence Depth/Lift

Effect of Liquid Viscosity
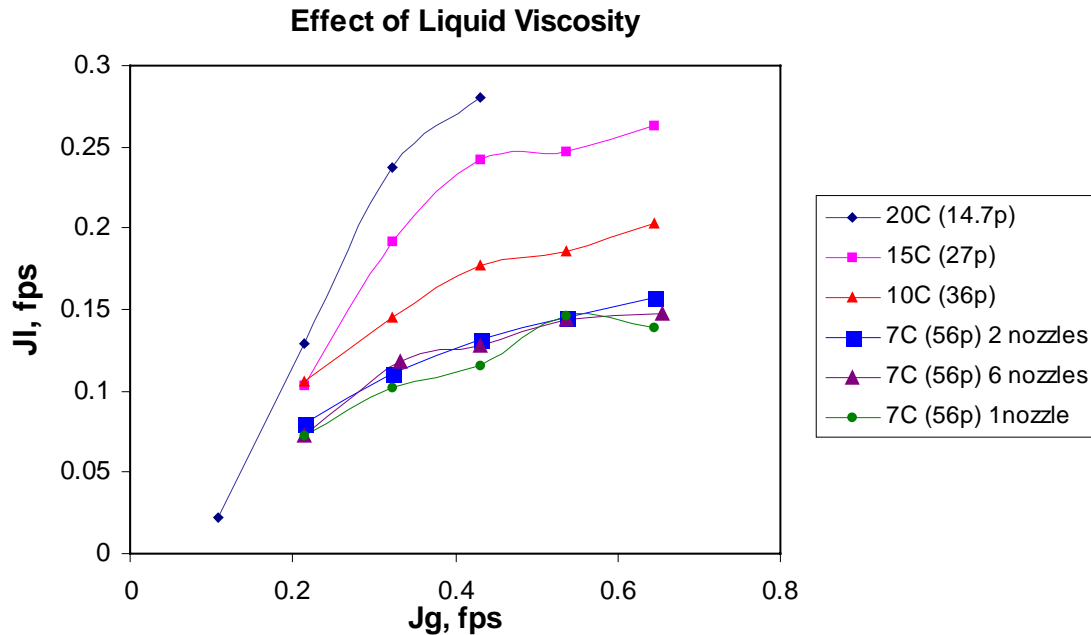
Figure 18   Liquid Superficial Velocity vs. Gas Superficial Velocity for
Varying Liquid Viscosities at Constant Submergence and Lift

The effect of liquid viscosity is illustrated in Figure 18, where the liquid capacity (in terms of superficial velocity) is plotted as a function of the gas velocity for a set of runs where the bubbler submergence and lift were held constant at 25-inches and 4-inches, respectively. The plot clearly shows that liquid flow increases as the viscosity decreases for the same airflow. This naturally follows from the decreased frictional pressure drop as viscosity decreases. The data for 7^oC were obtained with 1, 2, and 6 nozzles operating. The liquid flows were very similar for all three cases, with the one nozzle case just slightly below the other two cases.

This figure also shows that at low air flows, there is almost a linear increase in liquid flow with air flow. Then as the air flow is increased further, the slopes of the curves tend to decrease. Visual observations of the bubble flow pattern showed the bubbles coalescing and tending into a more disorganized structure at high air flows, no longer the regularly spaced bubble train image of the slug flow regime. If the air flow were increased further beyond where the void fraction equals 50%, then the annular regime would be reached, where the bubbles form a central core and very little liquid pumping is attained. Thus, a turning down of the liquid flow vs. air flow curve would be reached at a little bit higher air flow than those used in these tests.

6.5.2 Effect of Bubbler Submergence and Lift

Figure 19 gives the liquid capacity for various submergence depths (indicated by the label "S") and lifts (label "L"). The data shown are a subset where the liquid viscosity was in the range, 52

poise to 79 poise. The overall behavior can be characterized as an increase in liquid flow as the submergence depth is increased, if allowance for the effect of different liquid temperatures is taken into account. Compare for example the data for 27"S (for submergence), 4"L (for lift), 5.2^{o}C with the data for 14"S, 4"L, 5.1^{o}C. The increase in liquid flow with submergence depth may be explained by the increase in static driving head, $\Delta p_s = \alpha \rho g Z_s$ (See [1a]).

The effect of bubbler lift can also be obtained from Figure 19. Compare for example, the data for 16"S 9"L 7.6^{o}C with the data for 14"S 4"L 5.1^{o}C. Despite the smaller submergence depth and higher viscosity, the 14"S 4"L case has a higher liquid flow than the 16"S 4"L case. It is concluded that for the same submergence depth, a higher lift results in lower liquid flow. This is explained by the fact that the static pressure driving head in [1a] must overcome the static pressure drop due to lift.

The goal of this section is to collapse the data in Figures 18 and 19 to a single correlating equation, useful for design and for operational purposes. The target equation will be [4]. First, it will be necessary to evaluate the constants given in equations, [2]-[4], from the experimental data.

Effect of Airlift Bubbler Submergence and Lift
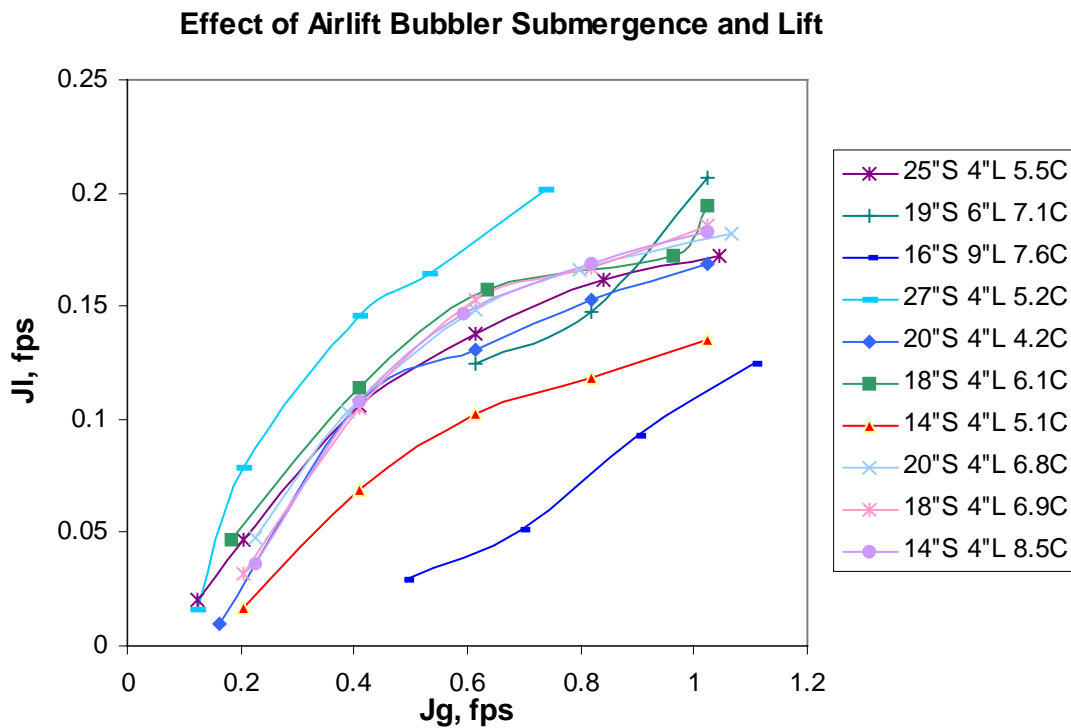
Figure 19   Liquid Superficial Velocity vs. Gas Superficial Velocity for
Various Airlift Bubbler Submergence Depths and Lifts

6.5.3 Bubble Rise Velocity

To use [4] the bubble parameters, C_o and V_t, must be evaluated from [3]. The void fraction was not measured directly during these tests. However, digital video recordings provided a means of obtaining the bubble rise velocity. This was achieved by advancing the recording frame by frame

and measuring the height the bubble traveled over the number of frames considered. The frame
speed was 30 frames/sec. The bubble rise velocity, with liquid flow, is actually the gas phase
velociy, $V_g = \dfrac{J_g}{\alpha}$. Then by plotting the phase velocity as a function of the mixture velocity
$J_m=(J_g+J_l)$, C_o and V_t can be obtained for a particular liquid viscosity.

Figure 20 plots the bubble rise velocity, V_g vs. J_m for glycerin temperatures, 7-21°C. The data
for 7°C (12 points) were curve fitted with a linear equation, where the coefficients correspond to
C_o=2.287 and V_t =0.247 fps.   The value for C_o agrees very well with the theoretical solution of
Collins, R, et. al, (Ref. 9.3) which was based on potential theory applied to laminar flow.
However, data for other temperatures indicate that C_o may change with viscosity. The number of
data points for the other temperatures were insufficient to obtain accurate measurement of C_o and
V_t at these conditions.
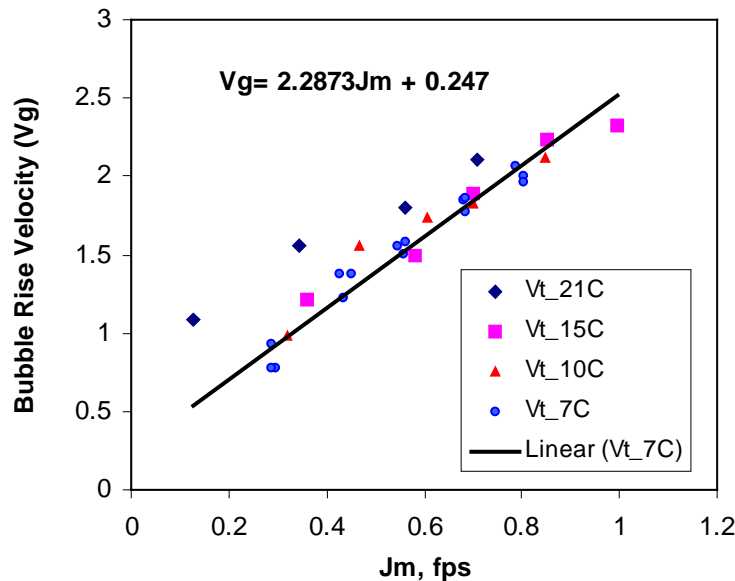
Figure 20 Bubble Rise Velocity at Various Mixture Velocities and Temperatures

Our procedure will then be to assume C_o=2.287 is correct and adjust the terminal velocity, V_t, for
different temperatures by using the correlation obtained by E. T. White and R. H. Beardman
(Ref. 4).
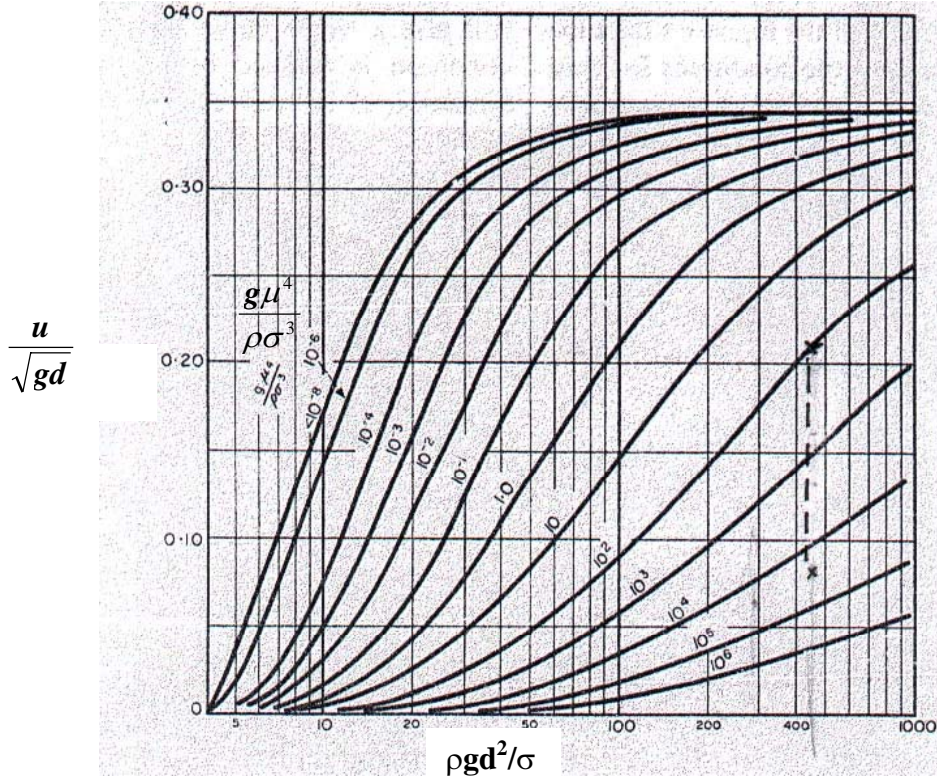
Figure 21   General Correlation for Bubble Rise of Cylindrical Air Bubbles in Stagnant
            Liquids in Vertical Tubes (White and Beardman, Ref. 9.4)

The bubble rise velocity of cylindrical air bubbles in stagnant liquids was measured and correlated by White and Beardman. Their correlation is reprinted in Figure 21. This bubble rise velocity thus corresponds to the terminal velocity V_t in [3]. For glycerin, $\rho g d^2 / \sigma = 450$ and

the range of the parameter, $\dfrac{g\mu^4}{\rho\sigma^3} = 3\text{x}10^4$ to 100, corresponding to $= 0.08$ to 0.21. White and

Beardman's parameter u corresponds to V_t. Using the chart in Figure 21, the calculated value for V_t at 7°C is 0.19 compared to our experimental value of 0.24.

6.5.4 Friction Factor

No experimental study of two-phase pressure drop in vertical tubes was found in our flow conditions which are in the laminar flow regime. We may use the laminar friction factor for single phase flow in tubes, $f = 64/\text{Re}$. However, for short liquid slugs between the air bubbles, the laminar velocity profile may not be fully developed and an exponent n in [2] different than 1 may be more applicable. To evaluate this exponent from the data, [1] is rewritten,

$$(\alpha - \frac{Z_l}{Z_t})/(J_m^{\,2}(1-\alpha)) = \frac{f}{2gD} = \frac{A}{2gD\,\text{Re}^n} = \frac{A}{2g\rho^n D^{n+1}}(\frac{\mu}{J_m})^n \qquad [5]$$

The left hand side will be defined as Par1.

For the data in Figure 22, where the bubbler geometry was held constant and liquid viscosity varied, the test points were plotted with (μ/J_m) as abscissa and Par1 as ordinate. The data is correlated with an exponent n=1.3326 with a correlation factor of R^2=0.798. This correlation is good only for cylindrical bubbles, where $J_g \geq 0.2\,fps$. For J_g<0.2 fps, the correlation of Figure 23 is obtained.

Correlation of Bubler Frictional Pressure Drop at Various Liquid Viscosities

Par1= 0.00095(μ/Jm)$^{1.33259}$
R^2 = 0.79831

Par1=(α−Zl/Zt)/((1-α)Jm^2)

μ/**Jm**
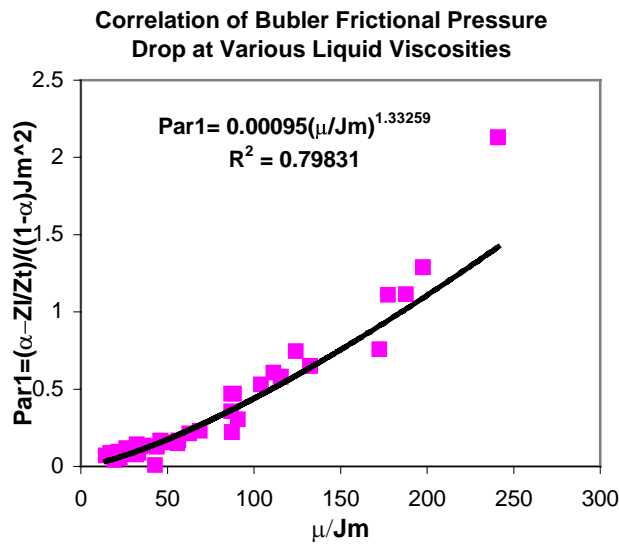
Figure 22   Correlation of Bubbler Frictional Pressure Drop at Constant Submergence and Lift and Different Temperatures, $J_g \geq 0.2\,fps$

Frictional Pressure Drop for Spherical Bubbles

Par1 = 0.0012(μ/Jm)$^{1.4703}$

Par1=(α-Zl/Zt)/((1-α)Jm^2)

μ/**Jm**
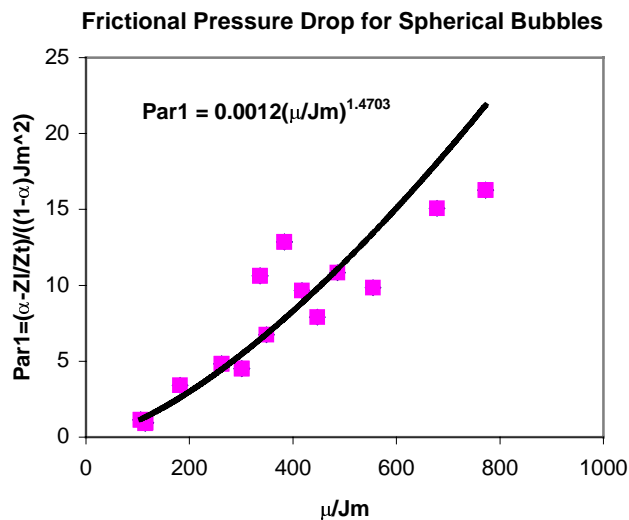
Figure 23 Correlation of Bubbler Frictional Pressure Drop for J_g<0.2 fps

When the effects of bubbler submergence depth and lift are included, the correlation for the frictional pressure drop is given in Figure 24. The correlation is based on 104 points, which are listed in Appendix A. The correlation is valid for $J_g \geq 0.2\,fps$. The exponent of (μ/J_m) is then used in [5], to write the friction factor as,

$$f = \frac{11.6}{Re^{1.246}} \qquad [6]$$

Overall Correlation of Frictional Pressure Drop for all Temperatures and Bubbler Lengths (Cylindrical Bubbles)
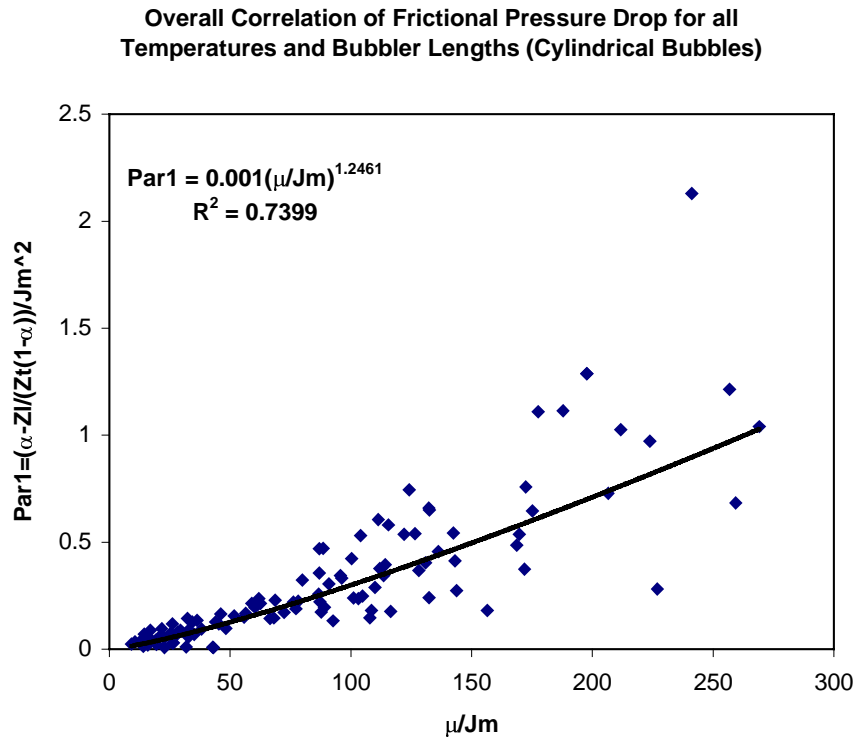
Figure 24 Correlation of Frictional Pressure Drop Over All Data with Varying Viscosity, Submergence Depth and Lift, for $J_g \geq 0.2\,fps$

6.5.5 Overall Design Equation

We now apply the friction factor, [6] , the coefficient $Co=2.287$, and bubble terminal velocity V_t, as evaluated from the chart of Figure 21, to the overall correlating equation, [4]. This equation relates the mixture velocity to gas velocity. Since the gas velocity is known, the only unknown is the mixture velocity. (The friction factor is also a function of J_m). Thus, the liquid velocity may be obtained from the mixture velocity. All of the data with $J_g>0.2$ fps are plotted in Figure 25. The right hand side of [4] is defined as Par2. If the design equation is valid, J_g=Par2. The curve fit shows the data to be within three percent of the design equation, with R^2=0.96. Thus, the liquid velocity may be predicted for a given gas velocity when bubbler submergence depth (Z_s) and lift (Z_l), liquid viscosity and tube diameter are known. It must be remembered that the coefficients for the frictional pressure drop correlation were obtained only for a subset of the data, $J_g>0.2$ fps, while the points on Figure 25 included all data. Also, the coefficients for the Drift Flux Equation used in the correlation were based only on the 6-7°C data. Nevertheless, the correlating equation still provides a good fit to the data.

Overall Correlation of Mixture Velocity vs. Gas Velocity

Par2 = 1.0285Jg
R^2 = 0.9627

Par2=(2.3Jm+Vt)(1-Zs/(Zt(1+fJm^2/2gD))

Jg
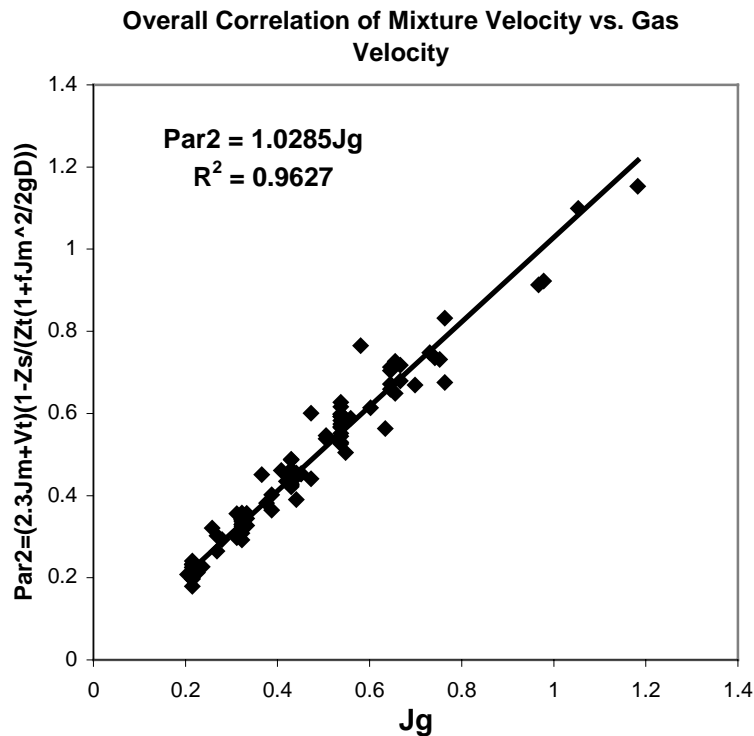
Figure 25   Test of the Design Equation [4] against the Experimental Data

6.5.6 Predicted Glass Flows

Using the design equation [4], a plot of predicted glass flows in hot glass may be predicted. Assume a viscosity of 60 poise, surface tension of 300 dynes/cm, a 24-inch submergence depth, 2.4-inch hydraulic diameter and exit slot bottom level with the glass surface. Since we did not measure the hydraulic resistance of the exit slots (which act like a weir and tends to raise the level of the glass inside the bubbler), we will assume a lift of 6-inches. This would be conservative, since a maximum liquid rise of about 3-inches above the slots were observed during tests where the slots were level with the surface and the flow catcher was not installed. To extend the glycerin results to glass, we use White and Beardman's correlation to determine the bubble rise velocity in glass. All other effects such as friction, which depends on viscosity,

are similar to the glycerin parameters. For glass, $\rho g d^2 / \sigma = 303$ and $\dfrac{g\mu^4}{\rho\sigma^3} = 188$. From Fig. 21,

$\dfrac{u}{\sqrt{gd}} = 0.16$. Thus, u or $V_t = 0.406$ ft/sec.

A plot of the predicted glass flow vs. injected airflow (inside the bubbler) is provided in Figure 26. Here, for a nominal airflow of 1.2 cfm, the predicted flow is 2450 lbs/hr.
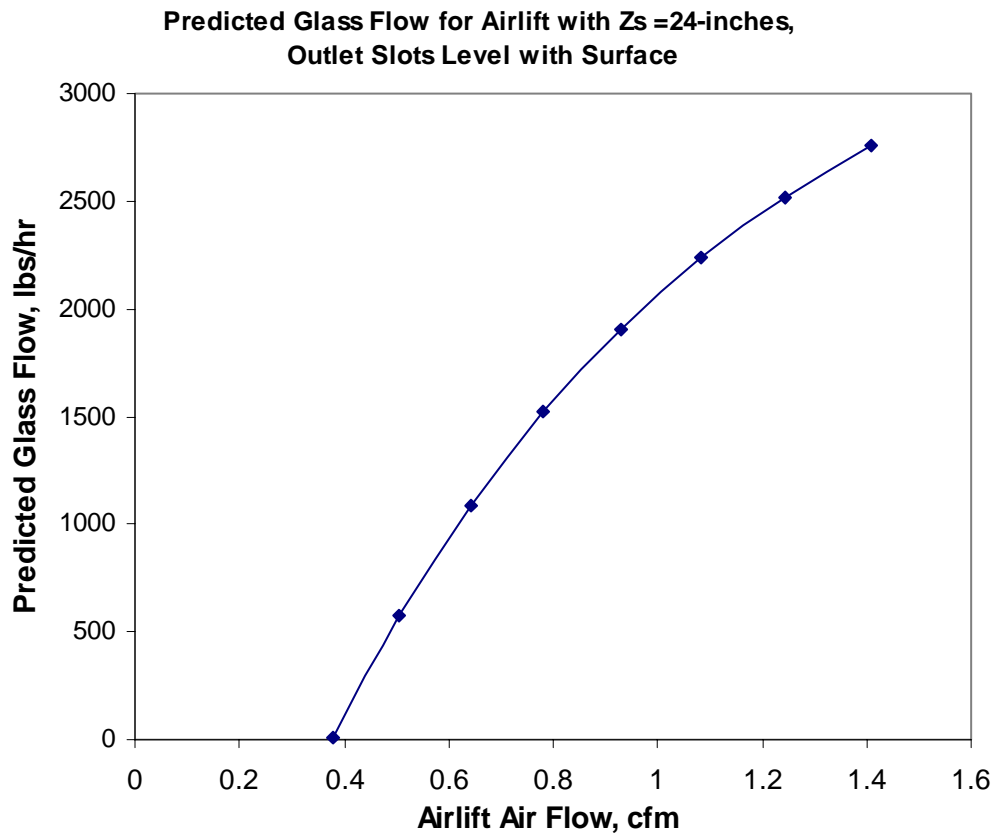
Figure 26   Predicted Glass flows for Airlift Bubbler with 24-inch Submerged Depth, Outlet Slots Level with Surface of Glass and with 60 poise Viscosity

7.0 Conclusions

A full-scale Plexiglas model of the Airlift Bubbler intended for installation in the DWPF Melter was tested in glycerin. The following conclusions are evident from the test results:

- The liquid flow pumped increases monotonically with airflow, over the range 0.2 to 1.2 scfm.
- Increasing the liquid viscosity decreases the pumped liquid flow for the same airflow.
- The number of nozzles has little effect on the pumping capacity.
- For the air flows tested, the "zone of influence" of the bubbler extends to the maximum width of the tank, 3 ft, and 6 to 12 inches below the bubbler opening.
- The optimum location of the bottom of the exit slots is within 2-inches, above or below the liquid surface, for maximum liquid flow (from the data) and high horizontal exit flow (visual results).
- A nominal glass flow of 2450 lbs/hr is predicted for a prototype airlift bubbler with a 24-inch submerged depth and for 60 poise glass viscosity at a bubbler air flow of 1.2 cfm. The actual operating flow would depend on other issues, such as erosion, plenum pressure spiking, and solids carryover.

8.0 Nomenclature

A_b – airlift flow area

A_o – orifice flow area

C – coefficient of friction factor relation, [2]

C_d – orifice discharge coefficient

C_o – distribution coefficient in Drift Flux Equation [3]

D – bubbler hydraulic diameter

f – friction factor

g – gravitational constant

h – liquid height inside flow catcher

J_l – superficial or average liquid velocity, Q_l/A

J_g – superficial or average gas velocity, Q_g/A

J_m – average mixture velocity, sum of J_l and J_g

Par1 – correlating parameter , $f/2gD=(\alpha-Z_l/Z_t)/(J_m^2(1-\alpha))$

Par2 – correlating parameter for J_g, $Par2 = [C_o J_m + V_t)][1 - \dfrac{Z_s}{(Z_s + Z_l)(1 + \dfrac{fJ_m^2}{2gD})}]$

Q_l – liquid volumetric flow rate

Q_g – gas volumetric flow rate

Re – bubbler Reynolds number based on mixture velocity

Reo – orifice Reynolds number

V_g – gas phase velocity or bubble rise velocity

Z_c – height of liquid in flow catcher (Tables 1 and 2)

Z_e- elevation of outlet slot bottoms above liquid surface

Z_l – bubbler lift or elevation of two-phase mixture above liquid surface

Z_s – submergence depth or distance from bubbler opening to liquid surface

Z_t- sum of Z_s and Z_l

α – void fraction

μ – viscosity

ρ – liquid density

σ – surface tension

9.0 References

1. WSRC-TR-2002-00196 Rev. 0, "DWPF Melter Air-Lift Bubbler: Development and Testing for Increasing Glass Melt Rates and Waste Dissolution", by H. N. Guerrero and. D. F. Bickford, to be issued.
2. Griffith, P. and Wallis, G.B., "Two-phase Vertical Slug Flow," J. Heat Transfer, Vol. 83, 1961, pp. 307-312.
3. Collins R. et. al. , "The motion of large gas bubbles rising through liquid flowing in a tube", Journal of Fluid Mechanics, Vol. 89, Part. 3, (1978), pp. 487-514.
4. White, E. T. and R. H. Beardman, "The velocity of rise of single cylindrical air bubbles through liquids contained in vertical tubes", Chemical Engineering Science, Vol. 17, (1962), pp. 351-361.

Appendix A
Airlift Bubbler Glycerin Data Tables

Table1
Airlift Bubbler Data and Correlating Parameters for $J_g \geq 0.2\,fps$

Date	Zs in.	Ze, in.	Airflow, scfm	T2, oC	Zc, in.	Zl, in.	μ, poise	Jg, fps	Jl, fps	Vt, fps	α	μ/Jm	Par1	Par2
6/25/02	24	3.75	0.59	21	3	5	15.9	0.312	0.180	0.477	0.200	32.30	0.1429	0.2922
	24	3.75	0.74	21	3.5	5.25	15.9	0.387	0.220	0.477	0.214	26.17	0.1178	0.3568
	24	3.75	0.90	21	4	5.5	15.9	0.473	0.260	0.477	0.226	21.67	0.0963	0.4310
	24	3.75	1.21	21	4.5	5.75	15.9	0.634	0.300	0.477	0.251	17.00	0.0876	0.5490
	24	3.75	1.45	21	5	6	15.9	0.763	0.339	0.477	0.263	14.40	0.0702	0.6573
6/26/02	29	3	0.51	16	4.5	5.5	17.3	0.269	0.275	0.462	0.162	31.77	0.0104	0.2948
	29	3	0.78	16	5.5	6.75	17.3	0.408	0.349	0.462	0.192	22.82	0.0068	0.4496
	29	3	0.96	16	6	7	17.3	0.505	0.385	0.462	0.209	19.40	0.0226	0.5318
	29	3	1.27	16	6.5	8	17.3	0.666	0.422	0.462	0.233	15.88	0.0188	0.6987
	29	3	1.45	16	7	8.5	17.3	0.763	0.459	0.462	0.242	14.14	0.0138	0.8099
	25	4	0.51	14.6	3.5	5	20.3	0.269	0.172	0.427	0.192	46.09	0.1648	0.2591
	25	4	0.72	14.6	4.5	5.75	20.3	0.376	0.234	0.427	0.213	33.26	0.0871	0.3724
	25	4	0.86	14.6	5	6	20.3	0.451	0.265	0.427	0.225	28.32	0.0796	0.4403
	25	4	1.15	14.6	5.5	7	20.3	0.602	0.297	0.427	0.250	22.59	0.0523	0.5976
	25	4	1.39	14.6	6	7.5	20.3	0.731	0.328	0.427	0.265	19.18	0.0418	0.7273
	25	4	0.41	11.95	3.5	5.5	29.2	0.215	0.120	0.338	0.200	87.24	0.2222	0.2190
	25	4	0.63	12	5	6	29.0	0.333	0.186	0.340	0.225	55.80	0.1498	0.3338
	25	4	0.84	11.3	5.25	7	32.0	0.441	0.178	0.316	0.263	51.67	0.1554	0.4328
	25	4	1.33	11.07	6.25	7.25	33.0	0.699	0.211	0.308	0.303	36.32	0.1346	0.6420
	25	4	1.86	9.67	6.75	7.5	40.1	0.978	0.190	0.264	0.345	34.35	0.1282	0.8755
	25	4	0.45	9.8	4	5.5	39.4	0.236	0.105	0.268	0.232	115.56	0.5809	0.2186
	25	4	0.59	9.86	5	6	39.1	0.312	0.138	0.270	0.248	86.94	0.3554	0.2951
	25	4	0.86	9.96	5.75	7	38.6	0.451	0.164	0.273	0.277	62.60	0.2137	0.4354
	25	4	1.27	10.1	6.5	8	37.8	0.666	0.193	0.277	0.307	44.02	0.1272	0.6519
	25	4	2.01	9.62	7.5	9	40.4	1.053	0.212	0.263	0.346	31.92	0.0774	1.0487
	25	4	0.43	9.11	4.188	5.5	43.3	0.226	0.101	0.248	0.234	132.53	0.6512	0.2103
	25	4	0.61	9.2	5.75	6.25	42.7	0.322	0.148	0.251	0.251	90.81	0.3049	0.3172
	25	4	0.84	9.45	6	7	41.3	0.441	0.161	0.258	0.279	68.69	0.2291	0.4282
	25	4	1.02	9.6	6.5	7.5	40.5	0.537	0.180	0.262	0.292	56.45	0.1680	0.5288
	25	4	0.41	5.85	3.625	5	65.3	0.215	0.056	0.174	0.279	241.06	2.1297	0.1697
	25	4	0.61	5.24	4.75	6	70.1	0.322	0.072	0.163	0.312	177.54	1.1099	0.2755
	25	4	0.84	5.85	5.125	6	65.3	0.441	0.085	0.174	0.331	124.19	0.7450	0.3671
	25	4	1.04	5.7	5.5	6.5	66.4	0.548	0.091	0.171	0.348	104.01	0.5309	0.4739
7/12/02	19	6	0.61	5.97	3.75	7	64.4	0.322	0.059	0.176	0.317	168.68	0.4854	0.3334
	19	6	0.82	6.02	4.25	7.25	64.0	0.430	0.069	0.177	0.337	128.14	0.3681	0.4414
	19	6	1.02	6.09	5.25	7.5	63.4	0.537	0.090	0.179	0.345	101.14	0.2395	0.5657
	16	9	0.49	7.09	1.375	9	56.2	0.258	0.014	0.199	0.324	206.48	0.7286	0.3147
	16	9	0.70	7.09	1.875	9.5	56.2	0.365	0.025	0.199	0.345	143.73	0.2735	0.4410
	16	9	0.90	7.09	2.75	10	56.2	0.473	0.045	0.199	0.353	108.43	0.1804	0.5851
	16	9	1.11	7.14	3.25	11	55.8	0.580	0.057	0.200	0.362	87.61	0.1740	0.7452
	27	4	0.41	7.35	5.06	6	54.4	0.215	0.101	0.204	0.239	172.37	0.7584	0.2061
	27	4	0.53	7.4	5.75	7	54.0	0.279	0.117	0.206	0.259	136.19	0.4562	0.2801
	27	4	0.74	6.7	6.75	7.5	58.9	0.387	0.129	0.191	0.292	114.22	0.3948	0.3815
	20	4	0.41	5.22	4	5.5	70.2	0.215	0.059	0.163	0.281	256.76	1.2137	0.2075
	20	4	0.61	5.26	5	6.25	69.9	0.322	0.077	0.164	0.309	175.05	0.6457	0.3210
	20	4	0.82	5.45	5.75	6.75	68.4	0.430	0.093	0.167	0.327	130.91	0.4034	0.4378
	20	4	1.02	5.6	6.25	7.5	67.2	0.537	0.104	0.170	0.340	104.85	0.2484	0.5695
	18	4	0.41	5	3.75	5.5	72.0	0.215	0.053	0.159	0.287	269.07	1.0409	0.2163
	18	4	0.63	5.29	5	6	69.7	0.333	0.077	0.164	0.312	169.76	0.5364	0.3412
	18	4	0.96	5.63	5.25	6.5	67.0	0.505	0.085	0.170	0.344	113.48	0.3439	0.5124
	18	4	1.02	5.83	5.75	7	65.4	0.537	0.097	0.174	0.342	103.16	0.2362	0.5706
	14	4	0.41	5.79	2.75	5	65.7	0.215	0.039	0.173	0.294	259.31	0.6834	0.2257
	14	4	0.61	5.83	3.75	5.5	65.4	0.322	0.058	0.174	0.319	171.94	0.3740	0.3447
	14	4	0.82	5.78	4.25	6	65.8	0.430	0.067	0.173	0.339	132.35	0.2407	0.4681

Date	Zs, in.	Ze, in.	Airflow, scfm	T2, oC	Zc, in.	Zl, in.	μ, poise	Jg, fps	Jl, fps	Vt, fps	α	μ/Jm	Par1	Par2
	14	4	1.02	5.73	4.75	6.5	66.2	0.537	0.077	0.172	0.353	107.83	0.1470	0.6026
	20	4	0.39	6.7	3.5	5.5	58.9	0.204	0.059	0.191	0.265	223.78	0.9716	0.2000
	20	4	0.61	6.79	4.75	6	58.3	0.322	0.087	0.192	0.295	142.37	0.5429	0.3159
	20	4	0.80	6.84	5.25	6.5	57.9	0.419	0.098	0.193	0.315	111.92	0.3775	0.4157
	20	4	1.06	6.84	5.75	7	57.9	0.559	0.109	0.193	0.336	86.69	0.2584	0.5610
	18	4	0.41	6.94	3.25	5	57.2	0.215	0.055	0.196	0.272	211.67	1.0259	0.2060
	18	4	0.61	6.85	4.5	6	57.9	0.322	0.082	0.194	0.297	143.01	0.4130	0.3314
	18	4	0.82	6.89	5	6.5	57.6	0.430	0.094	0.194	0.319	109.99	0.2897	0.4446
	18	4	1.02	6.94	5.5	7	57.2	0.537	0.105	0.196	0.334	89.05	0.1960	0.5677
	14	4	0.41	6.9	2.5	5.25	57.5	0.215	0.039	0.195	0.286	226.82	0.2813	0.2343
	14	4	0.59	6.81	3.5	5.75	58.1	0.312	0.060	0.193	0.308	156.46	0.1812	0.3447
	14	4	0.82	6.71	4.25	6	58.9	0.430	0.075	0.191	0.330	116.50	0.1758	0.4714
	14	4	1.02	6.85	4.75	6.25	57.9	0.537	0.088	0.194	0.343	92.58	0.1320	0.5930
	25	4	0.41	19.6	2.25	5.25	14.8	0.215	0.129	0.487	0.173	43.04	0.0067	0.2289
	25	4	0.61	19.6	3.5	5.5	14.8	0.322	0.236	0.487	0.188	26.49	0.0301	0.3352
	25	4	0.82	19.8	4	5.75	14.9	0.430	0.277	0.487	0.211	21.04	0.0596	0.4184
	25	4	1.02	19.87	4.75	6	14.9	0.537	0.340	0.486	0.222	16.99	0.0480	0.5183
	25	4	1.43	19.9	5.75	6.5	14.9	0.752	0.425	0.486	0.245	12.68	0.0365	0.7132
	25	4	1.84	20	6	7	15.0	0.967	0.444	0.486	0.269	10.61	0.0347	0.8891
	25	4	2.25	20.2	6.25	8	15.1	1.182	0.461	0.484	0.288	9.19	0.0239	1.1234
	25	4	0.43	11.75	3.438	5	30.0	0.226	0.114	0.331	0.210	88.47	0.4708	0.2066
	25	4	0.61	11.9	4.56	6	29.4	0.322	0.164	0.336	0.229	60.36	0.1948	0.3157
	25	4	0.84	12.85	5.438	6.5	25.7	0.441	0.231	0.369	0.239	38.25	0.0935	0.4415
	25	4	1.02	12.75	6	6.75	26.1	0.537	0.255	0.366	0.255	32.88	0.0899	0.5268
	25	4	1.25	12.47	6.5	7	27.1	0.656	0.269	0.356	0.274	29.32	0.0896	0.6256
	25	4	1.41	12.7	6.75	7.25	26.2	0.742	0.290	0.364	0.282	25.45	0.0744	0.7089
2 noz	25	4	0.41	19.4	2.25	5.25	14.7	0.215	0.129	0.488	0.173	42.80	0.0091	0.2292
8/5/02	25	4	0.61	19.3	3.5	5.5	14.7	0.322	0.237	0.488	0.188	26.28	0.0284	0.3358
	25	4	0.82	19.4	4	5.75	14.7	0.430	0.280	0.488	0.210	20.75	0.0572	0.4196
15C	25	4	0.41	12.33	3	5	27.7	0.215	0.103	0.351	0.205	86.92	0.4704	0.1979
8/5/02	25	4	0.61	13.1	4.5	6	24.8	0.322	0.192	0.378	0.214	48.29	0.0970	0.3315
	25	4	0.82	13.47	5.25	6.5	23.6	0.430	0.242	0.391	0.230	35.10	0.0682	0.4406
	25	4	1.02	12.85	5.75	7.5	25.7	0.537	0.247	0.369	0.257	32.78	0.0565	0.5573
	25	4	1.23	12.95	6	7.5	25.3	0.645	0.263	0.373	0.272	27.93	0.0691	0.6382
10C	25	4	0.41	10.5	3.75	5	35.8	0.215	0.106	0.290	0.216	111.37	0.6063	0.1958
8/6/02	25	4	0.61	10.2	5	6	37.3	0.322	0.144	0.280	0.247	79.88	0.3232	0.3050
	25	4	0.82	10.5	5.75	6.5	35.8	0.430	0.177	0.290	0.265	58.93	0.2146	0.4083
	25	4	1.02	9.08	6.375	7	43.4	0.537	0.164	0.247	0.300	61.92	0.2360	0.5016
	25	4	1.23	10	6.875	8	38.3	0.645	0.203	0.274	0.302	45.25	0.1179	0.6440
7C 2 noz	25	4	0.41	7.2	4.25	5.5	55.4	0.215	0.080	0.201	0.253	187.78	1.1142	0.1928
8/7/02	25	4	0.61	7.3	5.5	6.5	54.7	0.322	0.110	0.203	0.279	126.51	0.5402	0.3053
	25	4	0.82	7.4	6.375	7.25	54.0	0.430	0.132	0.206	0.298	96.16	0.3311	0.4207
	25	4	1.02	7.5	6.875	8	53.4	0.537	0.146	0.208	0.314	78.13	0.2244	0.5407
	25	4	1.23	7.5	7.375	9	53.4	0.645	0.157	0.208	0.327	66.51	0.1434	0.6797
7C 6 noz	25	4	0.41	7	4	5.5	56.8	0.215	0.073	0.197	0.259	197.57	1.2877	0.1885
8/7/02	25	4	0.63	7.25	5.875	6.25	55.1	0.333	0.118	0.202	0.279	122.03	0.5369	0.3115
	25	4	0.82	7.5	6.125	7.25	53.4	0.430	0.128	0.208	0.300	95.69	0.3437	0.4167
	25	4	1.02	7.6	6.75	8.5	52.7	0.537	0.144	0.210	0.314	77.28	0.1898	0.5562
	25	4	1.25	7.3	7.125	9.25	54.7	0.656	0.148	0.203	0.333	68.11	0.1454	0.6929
7C 1 noz	25	4	0.41	7	4	5.5	56.8	0.215	0.073	0.197	0.259	197.57	1.2877	0.1885
8/8/02	25	4	0.61	7.1	5.25	6.25	56.1	0.322	0.102	0.199	0.285	132.27	0.6592	0.2936
	25	4	0.82	7.3	5.75	7	54.7	0.430	0.116	0.203	0.306	100.26	0.4231	0.4014
	25	4	1.02	7.7	6.75	8	52.0	0.537	0.146	0.212	0.313	76.10	0.2201	0.5392
	25	4	1.23	7	7	9	56.8	0.645	0.140	0.197	0.335	72.42	0.1730	0.6709

Table 2
Airlift Bubbler Data and Correlating Parameters for $J_g<0.2$ fps

Date	Zs, in.	Ze, in.	Airflow, scfm	T2, oC	Zc, in.	Zl, in.	μ, poise	Jg, fps	Jl, fps	Vt, fps	α	μ/Jm	Par1	Par2
6/26/02	25	4	0.25	14.6	1.75	4.75	20.3	0.129	0.062	0.427	0.152	106.06	0.2439	0.1354
6/27/02	25	4	0.16	11.95	1	4.5	29.2	0.086	0.011	0.338	0.156	301.28	0.4471	0.0840
6/27/02	25	4	0.18	9.67	1	4	40.1	0.097	0.008	0.264	0.196	383.39	6.5548	0.0682
7/9/02	25	4	0.23	9.01	2.438	4.75	43.8	0.118	0.049	0.246	0.193	262.51	1.4735	0.0979
7/11/02	25	4	0.12	6.8	1.25	4.5	58.2	0.064	0.011	0.193	0.180	772.41	5.8715	0.0547
	25	4	0.20	9.9	1	4.5	38.9	0.107	0.008	0.271	0.205	336.18	4.8908	0.0801
	27	4	0.12	9.3	1.188	4	42.2	0.064	0.013	0.254	0.152	543.14	4.4784	0.0548
	27	4	0.20	7.2	3	4.5	55.4	0.107	0.051	0.201	0.195	348.53	2.5680	0.0787
7/17/02	20	4	0.16	5.12	1	4.5	71.1	0.086	0.004	0.161	0.239	785.75	8.8314	0.0662
	18	4	0.18	5.05	1.25	5	71.6	0.097	0.009	0.160	0.247	678.50	3.4665	0.0853
	14	4	0.20	5.88	1.25	4.5	65.0	0.107	0.010	0.175	0.248	554.92	0.5088	0.1052
7/18/02	20	4	0.23	6.51	2	4.5	60.3	0.118	0.026	0.187	0.234	417.43	3.1655	0.0927
	18	4	0.20	6.56	1.5	4.5	60.0	0.107	0.016	0.188	0.234	486.09	2.9287	0.0918
	14	4	0.23	6.86	1.25	4.5	57.8	0.118	0.011	0.194	0.247	447.33	0.3207	0.1163
7/23/02	25	4	0.20	19.9	1	4.5	14.9	0.107	0.021	0.486	0.140	115.94	0.9015	0.1174
7/23/02	25	4	0.23	12.1	1.625	4.5	28.6	0.118	0.039	0.343	0.172	181.87	0.9374	0.1050
21C	25	4	0.20	19.4	1	4.5	14.7	0.107	0.022	0.488	0.139	114.16	0.9261	0.1177